The effects of oxygen on charge transport in PDATS

1992 J. Phys.: Condens. Matter 4 2533

(http://iopscience.iop.org/0953-8984/4/10/016)

J. Phys.: Condens. Matter 4 (1992) 2533–2542. Printed in the UK

The effects of oxygen on charge transport in PDATS

N E Fisher† and D J Willock‡

† Department of Physics, King's College London, Strand, London WC2R 2LS, UK
‡ Chemistry Department, University College London, Christopher Ingold Laboratories, 20 Gordon Street, London WC1H 0AJ, UK

Received 17 October 1991

Abstract. We examine the effect oxygen contamination has on the recombination centre separation, trap density and defect ionization efficiency in PDATS single crystals. We find that, with no oxygen present, recombination centres are not detected in sample lengths of up to 9.8 mm. However, for those samples contaminated with oxygen, we find inter-centre separations of only a few hundred microns. We also show that oxygen increases the trap density and the defect ionization efficiency. Finally, we demonstrate that by activating the oxygen present in the crystals, the recombination centre separation can be further reduced.

1. Introduction

PDATS (the polymer bis(*p*-toluene sulphonate) ester of 2,4-hexadiyne-1,6-diol) is easily produced as millimetre-sized single crystals in which the polymer backbone direction is well defined and common to all chains in the sample [1]. Because the chain separation is large (0.7 nm) compared with the repeat unit distance on a chain (0.45 nm) [2], each may be considered as an independent, quasi-one-dimensional semiconductor with a material band gap of 2.4 eV (see, e.g., [3, 4]). Dark-conductivity measurements along and perpendicular to the chains made by Siddiqui and Wilson show an anisotropy of over 1000 reflecting this one-dimensional nature [5]. Experiments on PDATS may, then, offer an insight into one-dimensional carrier motion.

However, after over a decade of work on the electrical properites of this material, agreement on the mode of carrier propagation, trap density and recombination centre separation distances has not yet been reached. For instance, in a series of photoconduction experiments Donovan and Wilson conclude that carriers travel along the polymer chains for up to 1 mm before encountering trapping centres (see, e.g., [6]) and that recombination centres are absent in all samples used (up to 5 mm in length) [7]. Other groups, in particular Bassler *et al* [8] and Moses and Heeger [9], have presented work that in their opinion indicates trapping centres to be present on the micron scale or less, work that is in broad agreement with time-of-flight experiments recently presented by us [10, 11]. In addition, the density of recombination centres has also been questioned by Frankevich *et al* [12]. They find recombination centres in sample lengths of less than 250 μm.

Because of these differing conclusions, we have looked at the effects of sample preparation and history, an important contributory factor being the effects of oxygen. The Raman spectroscopy group at QMWC have presented work that indicates that

0953-8984/92/102533+10$04.50

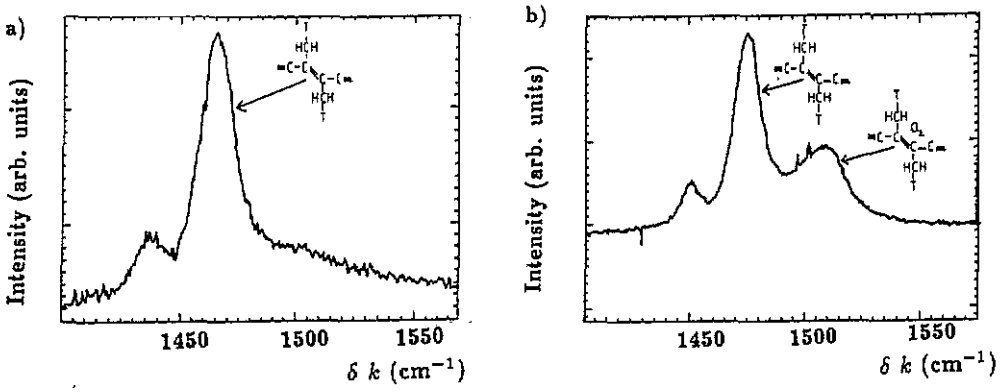

Figure 1. Example Raman Spectra from (a) an oxygen-free sample and (b) an oxygen-rich sample. The insets show the origins of the vibrational peaks. δk = change in wavenumber between incident and backscattered light.

PDATS can undergo chemical changes in the presence of oxygen (^{16}O) [13]. On comparing Raman spectra of samples held under vacuum with those kept in air an extra peak in the region of the double-bond stretching mode of the polymer chains is observed for the samples exposed to air (see, for example, figure 1). They propose that this secondary peak is due to molecular oxygen in defect sites modulating the natural vibrational frequencies of the polymer chain. This was confirmed by taking spectra of samples in the heavier isotope of oxygen, ^{18}O [14]. A shift in the secondary peak was observed.

In both cases the secondary peak could be reduced in magnitude by exposing the crystals to green light from an argon ion laser (photon energy 2.6 eV). Here it was found that the oxygen and the polymer chains take part in an 'ene' reaction (the oxygen is now activated) in which the chain becomes broken and one of the side groups forms P-toluenesulphonic acid [13]. The peak is reduced, and eventually lost, since the vibrational frequencies of the reaction products are not in the same range as the unbroken chain.

Two states of oxygen in the crystal are possible then: absorbed molecular oxygen giving rise to secondary peaks in the Raman spectra and activated oxygen giving rise to chain breaks.

To investigate these effects of oxygen on carrier propagation, two batches of crystals were prepared at the same time by the standard evaporation method from a solution of monomer in acetone [15]. The first, to be termed oxygen-free, was prepared from an acetone solution that had been de-gassed by passing nitrogen through it. The crystals were grown in a nitrogen environment and polymerized under vacuum. Hence, at all stages of preparation care was taken to eliminate oxygen contamination. For the other set, to be termed oxygen-rich, no such precautions were taken and all preparation steps took place in air.

Figure 1 shows example Raman spectra in the region of the double-bond stretching mode for each set of samples. These spectra confirm the designations of the samples although the actual quantity of oxygen present cannot be determined from these data.

2. Experimental arrangement

For the experiments presented here, the samples are contacted with either bulk electrodes consisting of silver-paste on the (011) face or additional surface electrodes evaporated onto the (100) face, as in figure 2. In each case the applied field lies in the chain direction. Following illumination of the (100) face, carriers are generated in the crystal which then propagate, in response to the electric field, along the chain direction. This gives rise to an induced photocurrent on the electrodes, which can then be observed using an amplifier and oscilloscope (Tektronix 7633) arrangement having an overall response time of 5 ns. To measure the induced charge on the electrodes, a Keithley 610C Coulombmeter and chart recorder are used in place of the amplifier and oscilloscope.

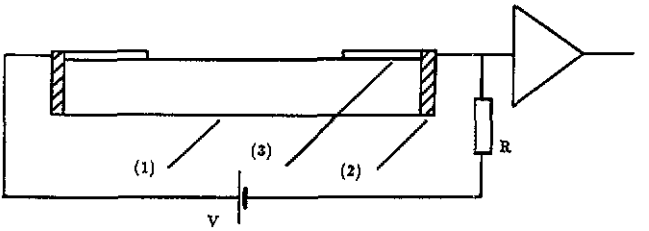

Figure 2. Sample electrode configuration. (1) PDATS sample. (2) Silver-paste bulk electrodes on the (011) face. (3) Evaporated Ag electrodes on the (100) face.

For all the experiments presented here samples were kept under a vacuum of 10^{-6} Torr for 24 h prior to readings being taken.

3. Results

3.1. Mono-molecular recombination

Here we compare the degree of mono-molecular recombination present for carriers generated in the oxygen-rich crystals with that for carriers generated in the oxygen-free crystals as follows. In a pulsed experiment the charge Q generated following a laser pulse is

$$Q = \frac{G\eta\phi}{E_{ph}} wlqT_L \tag{1}$$

where G is the incident laser intensity, $\eta\phi$ is the probability that a photon produces a free-carrier pair, l is the sample length, w is the sample width, q is the electronic charge, T_L is the duration of the light pulse, and E_{ph} is the photon energy. As this charge drifts a distance δx, it will induce a measured charge δQ_m on the electrodes which is given by

$$\delta Q_m = \frac{G\eta\phi}{E_{ph}} wlqT_L \frac{\delta x}{l} \tag{2}$$

If all the carriers traverse the sample length l, eventually to recombine at the electrodes, then $\delta x = l$ and therefore the measured charge Q_m is given by

$$Q_m = \frac{G\eta\phi}{E_{ph}} wqT_L l. \tag{3}$$

However, if the carriers encounter recombination centres of mean separation s_r, then $\delta x = s_r$ and thus the measured charge is now given by

$$Q_m = \frac{G\eta\phi}{E_{ph}} wqT_L s_r. \tag{4}$$

Using these equations then, the degree of carrier recombination can thus be determined by observing the dependence of the Q_m variable on l; Q_m will be independent of l if recombination centres are present within l, but will show linearity if recombination centres are absent from l.

The other important feature of these equations is the linearity of Q_m with light intensity. This is a characteristic of mono-molecular recombination (either at the electrodes and/or within the sample) and may be used to distinguish it from bimolecular recombination where a $G^{0.5}$ dependence would be expected.

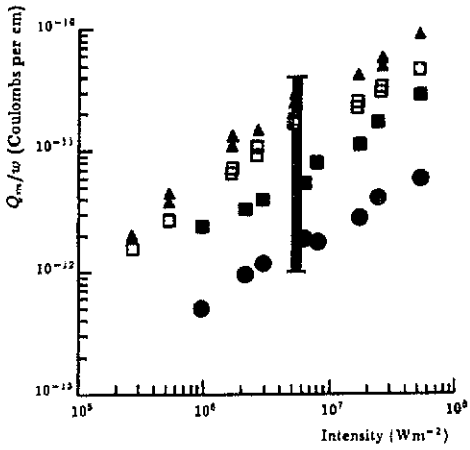

Figure 3. Intensity dependence of Q_m for the oxygen-free samples. The applied field is 2.6 x 10^4 V m^{-1}. Full triangles, l=9.18 mm. Open squares, l=3.78 mm. Full squares, l=2.40 mm. Full circles, l=0.24 mm. The vertical bar indicates the range of Q_m expected if Q_m scales with sample length.

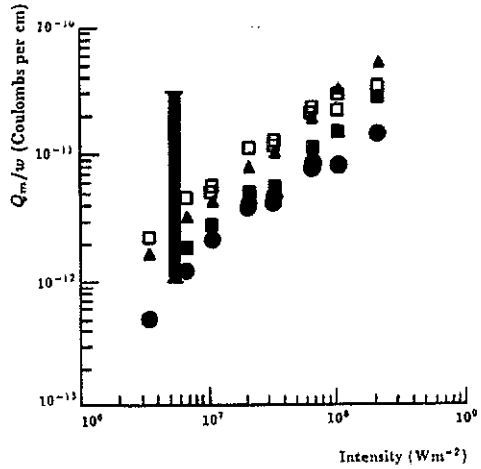

Figure 4. Intensity dependence of Q_m for the oxygen-rich samples. Applied field is 2.6 x 10^4 V m^{-1}. Open squares, l=1.64 mm. Full triangles, l=7.00 mm. Full squares, l=1.28 mm. Full circles, l=0.24 mm. The vertical bar indicates the range of Q_m expected if Q_m scales with sample length.

Figure 3 shows the intensity dependence of Q_m for the oxygen-free pair of samples and figure 4 shows that for the oxygen-rich pair, both following illumination with a 10 ns laser pulse of above-band-gap photon energy 3.68 eV, in a skin depth of 0.5 μm and an applied field of 2.6 x 10^4 V m^{-1}. By employing both bulk and surface

electrode geometries on each sample, these data were taken using effective sample lengths of 240 μm to 9.18 mm and 240 μm to 7.00 mm for the oxygen-free and oxygen-rich samples respectively. The vertical bars shown in the figures represent the range of Q_m expected if Q_m scales with the sample length, for the same light intensity. Hence, by reading the values Q_m from the position of the bars we are able to plot a length dependence of Q_m for both the oxygen-free and oxygen-rich samples that is at constant field and intensity. This is shown in figure 5. The first point to note is that the oxygen-free samples give linearity of Q_m with l, indicating that no recombination centres are present in these samples for up to l=9.18 mm. The oxygen-rich samples on the other hand have Q_m independent of l indicating that s_r in this case is less than the sample lengths used. By extrapolating the oxygen-rich data to the sample length at which their Q_m values would agree with the oxygen-free data, we may estimate the value of s_r for each oxygen-rich sample. From figure 5 this gives values of s_r of 900 μm and 350 μm for the two samples used.

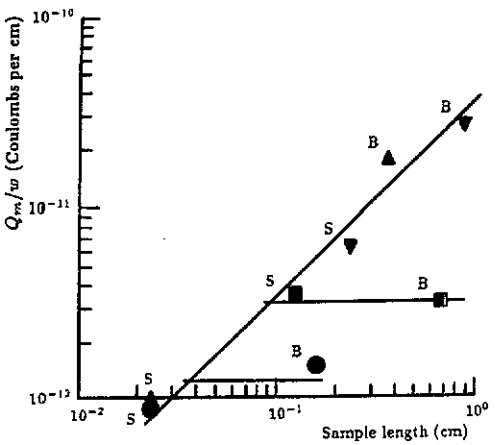

Figure 5. Length dependence of Q_m for the oxygen-free and the oxygen-rich samples. Inverted triangles, one oxygen-free sample. Triangles, the other oxygen-free sample. Squares, one oxygen-rich sample. Circles, the other oxygen-rich sample. Label S indicates surface electrodes used, and label B indicates bulk electrodes used.

3.2. Trapping

To observe the difference in trap concentrations due to the presence of oxygen, we can compare transit currents found using an oxygen-free crystal with those found using an oxygen-rich crystal.

The technique used is a surface configuration of the classic Kepler LeBlanc [16, 17] time-of-flight experiment, as illustrated in figure 6; by employing an optical mask, carrier generation is confined to a 60 μm strip near one electrode. After generation, carriers of one sign discharge at the nearest electrode while those of the other sign traverse, as a sheet, across the sample length. Hole or electron transits are expected, depending on the polarity of the applied field. In a perfect sample, all the carriers initially created arrive at the absorbing electrode as a localized sheet and then discharge, leading to a well defined transit edge. If, however, carriers undergo

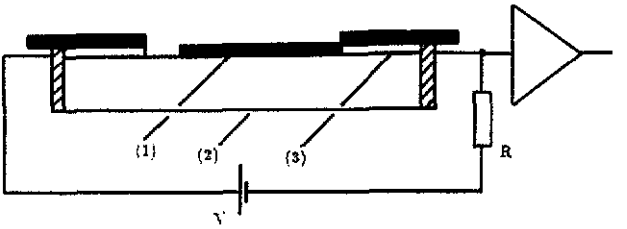

Figure 6. Arrangement for surface configuration transit current experiment. (1) Opaque optical mask with slit. (2) PDATS crystal. (3) Ag surface electrodes.

trapping, the arrival times become more spread out which can then lead to ill-defined transition regions and broad tails [18]. Carriers that become deeply trapped (i.e. held in traps whose retention time is greater than the timescale of the experiment) do not contribute further to the observed current and a general decay is superimposed on the transit profile.

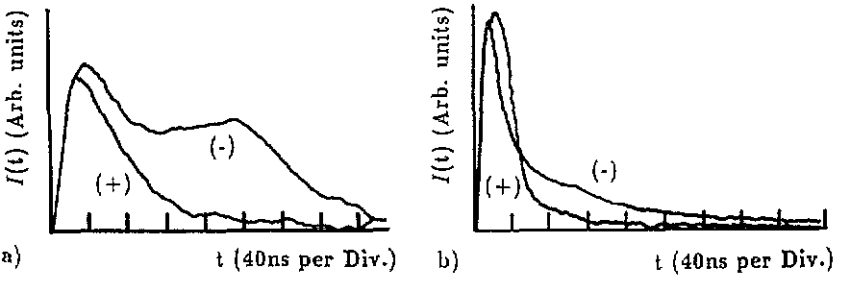

Figure 7. Transit currents obtained using: (a) an oxygen-free sample of length 240 μm with an applied field of about 2.9×10^6 V m^{-1} and (b) an oxygen-rich sample of length 240 μm with an applied field of about 8.3×10^6 V m^{-1}. (-) left electrode negative. (+) left electrode positive.

For a 10 ns laser pulse of photon energy 3.68 eV, figure 7 shows the transit signals obtained using an oxygen-free and oxygen-rich sample with in both cases the inter-electrode distances equal to 240 μm. Neither sample shows a hole transit, in agreement with earlier, exclusively oxygen-free experiments [10]. The oxygen-free sample (figure 7(a)) shows a clearly defined electron transit with relatively little dispersion. In addition we note that the magnitude of the current at the transit shoulder is around two thirds of the initial peak photocurrent. This ratio gives an indication of the fraction of carriers in the initial carrier packet that have become deeply trapped during the transit.

Electron transits in the oxygen-rich sample on the other hand (figure 7(b)) are only observed at the very highest applied fields (in excess of 5×10^6 V m^{-1}) and, as can be seen, the resulting transits are very dispersive. Also, the transition region is only one fifth of the initial peak photocurrent, so we can infer that both the deep- and the shallow-trap concentrations have been increased by the inclusion of the oxygen.

These conclusions are consistant with the photocurrent tails observed following illumination of the whole of the (100) face (uniform illumination). Again, using a 10 ns laser pulse of photon energy 3.68 eV incident on samples with bulk electrodes,

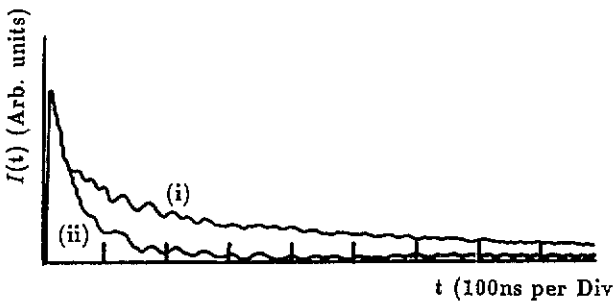

Figure 8. Comparison of uniform illumination photocurrents obtained using (i) an oxygen-free sample and (ii) an oxygen-rich sample. In both cases the sample length is about 8 mm and the applied field is about 7.5×10^4 V m^{-1}.

figure 8 shows the induced photocurrents. Here, the current with the narrower profile is obtained using an oxygen-rich sample while that with the broader profile is obtained using an oxygen-free sample. These differences in tail width indicate that the deep-trap density is higher in the oxygen-rich sample.

3.3. Defect ionization

Photoconduction in PDATS using below-band-gap illumination has been assigned to the ionization of defects [3]. To investigate the dependence of this process on oxygen contamination, we compare the Q_m data obtained using oxygen-rich crystals with that obtained using oxygen-free crystals. In order to confine the photon energies to below the band gap, a tungsten filament and Wratten filters are used which here gives photon energies less than 1.7 eV. Using a mechanical shutter, the light pulse duration is about 0.5 s. Because the skin depth of the below-band-gap photons will be greater than the crystal thickness, surface electrodes cannot be used and so a bulk electode configuration is employed.

We wish to know the dependence of the ionization efficiency $\eta\phi$ (which we now redefine as the probability that an incident photon will ionize a defect) with oxygen content. Inspection of equations (3) and (4) show that comparison may be made by—in the oxygen-free case—dividing the Q_m data by wl, or—in the oxygen-rich case—dividing Q_m data by ws_r. Here, the values of s_r are those deduced in section 3.1.

Figure 9 shows the intensity dependence of these adjusted Q_m values for the four samples used in section 3.1.

This figure shows that the oxygen-rich samples have a 30 times greater defect ionization probability. This suggests, therefore, that defect concentration is significantly increased by the presence of oxygen.

3.4. Activated oxygen and recombination length

This section investigates the dependence of s_r on the amount of activated oxygen present in a sample.

Figure 10(a) shows the Raman spectrum of a typical oxygen-rich sample. Figure 10(b) shows the new Raman spectrum, after exposure to green light of intensity about 1.5 μ W m^{-2} for 2 h. As can be seen, the secondary peak has been reduced, indicating (as described in section 1) an increase in the amount of activated oxygen.

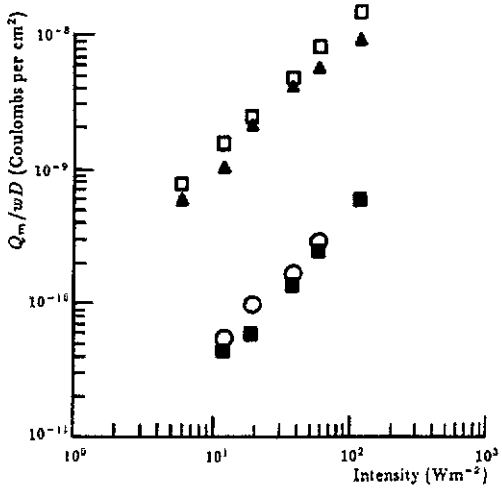

Figure 9. Comparison of the ionization efficiencies for the four samples used in section 3.1. Open squares and full triangles, the two oxygen-rich samples. Open circles and full squares, the two oxygen-free samples. Here $D = l$, for the oxygen-free samples and $D = s_l$, for the oxygen-rich samples.

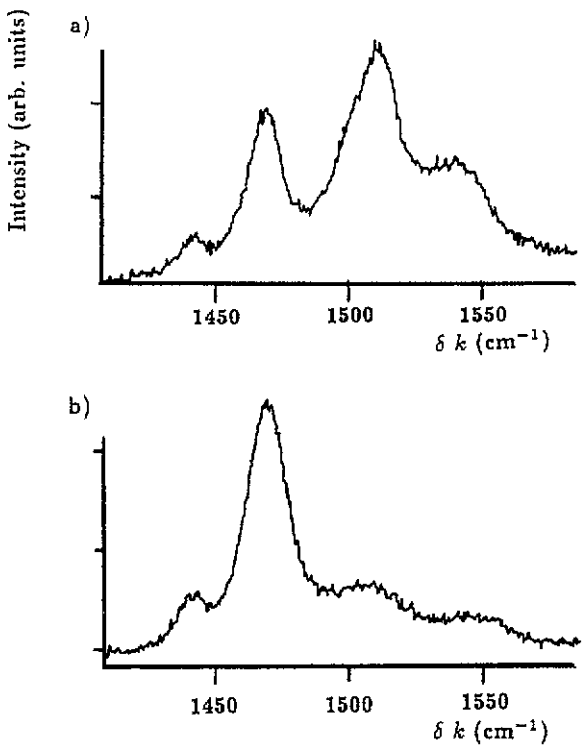

Figure 10. Activation of oxygen under exposure to green light: (a) Raman spectrum before exposure; (b) Raman spectrum after exposure.

By comparing the Q_m data using this sample before and after exposure to the

green light, any changes in the value of s_r (due to oxygen activation) will result in corresponding changes in Q_m.

In experiments, however, other factors may influence the value of Q_m after exposure to the green light (for example changes in crystal reflectivity). To check for this the peak photocurrent I_p immediately following a 10 ns laser pulse is also monitored, before and after the exposure. The reasons for this are as follows: I_p is a convolution of carrier density and carrier velocity. Since it is known from the transit current experiments [10] that the carrier velocities are at most about 3000 m s^{-1}, and since also s_r is about 300 μm then only a small fraction of the initial carrier density will recombine after 10 ns. Thus I_p, at a given field, is predominantly dependent on $\eta\phi$ only, which itself is dependent on sample reflectivity etc. So, if the value of I_p changes by some factor, then crystal reflectivity has also changed, and thus the Q_m data must be adjusted by that same factor in order to obtain meaningful comparisons.

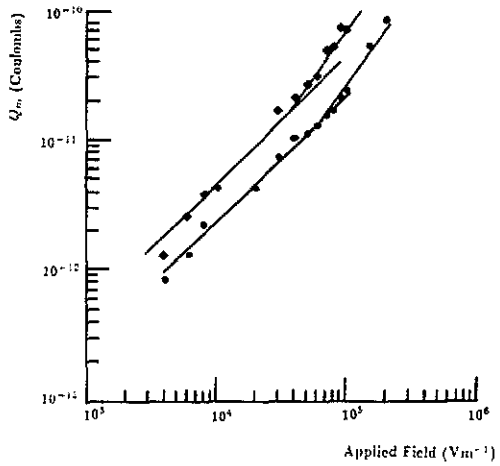

Figure 11. Field dependence of Q_m data before (diamonds) and after (circles) oxygen activation.

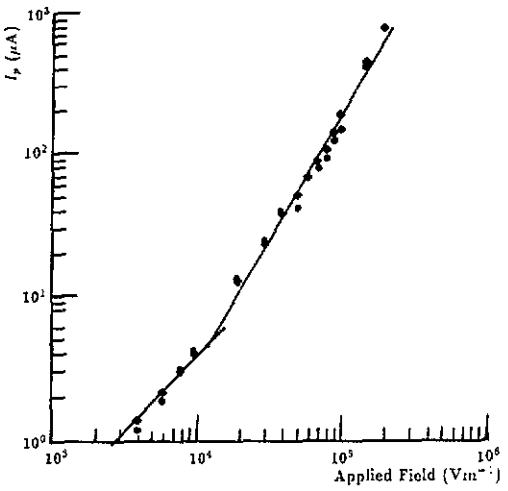

Figure 12. Field dependence of I_p data before (diamonds) and after (circles) oxygen activation.

As before, the following data are taken using a 10 ns laser pulse of photon energy 3.68 eV. Figure 11 shows the field dependence of Q_m before and after exposure. A factor of two change is observed. Further, figure 12 shows the field dependence of I_p before and after exposure. Here, no change is observed indicating, therefore, that the change in Q_m is due solely to changes in s_r.

Thus, we conclude that by activating oxygen we shorten s_r, in this case by a factor of two.

4. Conclusions

We have shown that oxygen when introduced in PDATS during the growth stage causes an increase in the defect concentration leading to the introduction of recombination centres and an increase in the trap density. Confirmation of this is evident from the observed increase in defect ionization probability for an oxygen-contaminated crystal.

In addition, we have found that on activating the oxygen in oxygen-rich crystals there is an increase in the recombination centre density. Because this process can occur even under normal ambient conditions, albeit very much more slowly, this can imply that these crystals may degrade further with age.

It should be noted that we have assumed throughout that the oxygen-free cystals are entirely devoid of oxygen. In fact, all PDATS crystals can be contaminated to some degree if left exposed to air. Thus realistically, even with oxygen-free samples, degradation of the crystals with age should be expected.

From these conclusions, we suggest that the 250 μm estimate for the s_r reported by Frankevich *et al* [12] indicates that their samples are contaminated with oxygen while those used by Donovan and Wilson [7], because of their reported absence of recombination centres, appear to be oxygen-free.

However, we find that even for the oxygen-free crystals the transit current experiments [10] still show that carrier transport is dominated by shallow trapping centres, possibly on all accessible length scales. This is in agreement with the conclusions of Bassler *et al* [8] and Moses *et al* [9] but is not reconcilable with the millimetre inter-trap separations claimed by Donovan and Wilson [6].

From this work then, we suggest that in order to study the intrinsic charge transport properties of PDATS samples, crystals need to be freshly grown, oxygen-free and if possible kept under vacuum to prevent oxygen contamination.

Acknowledgments

We thank Professor D N Batchelder (Leeds University (UK)) for many useful discussions during the course of this work.The experiments presented here were conducted at Queen Mary and Westfield College, London. This work was been supported by the SERC (UK).

References

[1] Bloor D 1980 *Recent Advances in Quantum Theory of Polymers* (Berlin: Springer) p 14
[2] Pope M and Swenberg C E 1982 *Electronic Processes in Organic Crystals (Monographs on Physics and Chemistry of Materials No 39)* (Oxford: Oxford Science Publications)
[3] Chance R R and Baughman R H 1976 *J. Chem. Phys.* **64** 3889
[4] Siddiqui A S 1980 *J. Phys. C: Solid State Phys.* **13** 2147
[5] Siddiqui A S and Wilson E G 1979 *J. Phys. C: Solid State Phys.* **12** 4237
[6] Donovan K J and Wilson E G 1985 *J. Phys. C: Solid State Phys.* **18** L51
[7] Donovan K J and Wilson E G 1981 *Phil. Mag.* B **44** 9
[8] Blum T and Bassler H 1981 *Chem. Phys.* **123** 431
[9] Moses D and Heeger A J 1989 *J. Phys. C: Solid State Phys.* **1** 7395
[10] Fisher N E and Willock D J 1991 *J. Phys. C: Solid State Phys.*
[11] Fisher N E 1990 *PhD Thesis* University of London
[12] Frankevich E L, Lymarev A A and Sokolik I A 1989 *J. Phys. C: Solid State Phys.* **1** 5545
[13] Poole N J and Day R J 1989 *Makromol. Chem.* **190** 2909
[14] Poole N J and Batchelder D N 1984 *Mol. Cryst. Liq. Cryst.* **105** 55
[15] Wegner G 1969 *Z. Naturf.* B **24** 824
[16] Kepler R G 1960 *Phys. Rev.* **119** 1226
[17] LeBlanc Jr O H 1960 *J. Chem. Phys.* **33** 626
[18] Scher H and Montroll E W 1975 *Phys. Rev.* B **12** 2455